Journal of Alloys and Compounds 488 (2009) 370–373

Contents lists available at ScienceDirect

Journal of Alloys and Compounds

journal homepage: www.elsevier.com/locate/jallcom

Preparation and near-infrared absorption of nano-SnO_2/SiO_2 assemblies with doping and without doping

Shujie Hai [a], Chunjie Yan [b,*], Hongjie Yu [a], Guoqi Xiao [a], Duo Wang [a]

[a] Faculty of Material Science and Chemical Engineering, China University of Geosciences, Lu Mo Road 388, Wuhan 430074, PR China
[b] Engineering Research Center of Nano-Geomaterials, Ministry of Education, China University of Geosciences, Lu Mo Road 388, Wuhan 430074, PR China

ARTICLE INFO

Article history:
Received 23 May 2009
Received in revised form 27 August 2009
Accepted 28 August 2009
Available online 2 September 2009

Keywords:
Oxide materials
Sol–gel processes
Nanostructured materials
Red shift

ABSTRACT

The assemblies of nano-SnO_2/SiO_2 and Sb- or Pd-doped nano-SnO_2/SiO_2, in which the nano-SnO_2 particles are located in the pores of mesoporous SiO_2 dry gels, were synthesized. Only for the Sb-doped nano-SnO_2/SiO_2 assemblies, a broad near-infrared absorption step occurs in the optical absorption spectrum of the wavelength range from 300 to 1500 nm. The near-infrared absorption phenomenon is attributed to electronic transitions from the ground states to the excitation states of the impurity energy levels, which are formed by Sb doping in SnO_2. With increasing the weight ratio of SnO_2:SiO_2 or the annealing temperature, the near-infrared absorption step slope side exhibits "red shift", which is caused by the quantum confinement effect weakening due to the increased SnO_2 crystalline diameter.

Published by Elsevier B.V.

1. Introduction

How to apply thermal energy is one of the significant research topic due to its wide applications, such as heaters and heat absorption coatings, etc. [1–6]. One of the key topics of thermal energy applications is to study and prepare new materials with high solar energy absorption and storing ability [7]. As we know, the mesoporous solids possess very high absorption ability to heat. In order to improve or modulate the thermal absorption ability of mesoporous solids, the assemblies of nano-particles with the mesoporous solids were designed [8–11]. The near-infrared absorption study of the assemblies of nano-particles with the mesoporous solids has been reported [12]. But the studies on the near-infrared absorption of Sb- and Pd-doped assemblies are very rare. As we know, the electrical, optical and magnetic properties of nano-materials can be modified by doping [13,14–19]. For example, to modulate the optical properties, different rare earth elements were used as dopant in materials [20–23]. Heo [24] observed that after Er or Tm doping in sulphide glasses, strong absorption peaks appeared in the visible and near-infrared wavelength range. However, the effect of non-rare earth element doping on the near-infrared absorption is scarcely reported. In this paper, we try to design Sb- and Pd-doped SnO_2/SiO_2 assemblies. The aim is to obtain the nano-SnO_2/SiO_2 assemblies with high near-infrared thermal absorption ability.

2. Experiments

2.1. Sample preparation

The nano-SnO_2/SiO_2 mesoporous assemblies were prepared by the following three steps. SiO_2 sol preparation: tetraethoxysilane (TEOS) was firstly mixed with ethyl alcohol (E_tOH) and distilled water. The molar ratio of TEOS:E_tOH:H_2O was 1:4:18. With constant stirring of the mixture, a dilute aqueous solution of HNO_3 (the concentration is 30 wt.%) was slowly added in the mixture until pH reached 2. After stirring for 100 min, the mixture solution became a uniform SiO_2 sol. SnO_2 sol preparation: $SnCl_4{\cdot}5H_2O$ was dissolved in the aqueous solution of E_tOH by stirring, the molar ratio of $SnCl_4$:E_tOH:H_2O was 1:2:8. Under stirring, aqueous ammonia was added in the mixed solution until pH 4–5, resulting in forming the SnO_2 sol. Nano-SnO_2/SiO_2 assemblies' preparation: the SnO_2 sol with different weights was mixed with a certain weight of SiO_2 sol by stirring for 30 min. Then, the mixed sol was sealed in a glassware and gelled within 3 days at 50 °C. After that, the wet gel was aged at 120 °C for 5 days. Finally, the wet gel was slowly heated from 50 to 120 °C, resulting in the dry gel forming. This gel was annealed in a 50% O_2 atmosphere at 300 °C for 2 h. The gel then was divided into several parts, and annealed at 400, 650, 800 and 900 °C for 1.5 h, respectively. Each part gel corresponds to annealed temperature. Through changing the weight ratio of SnO_2/SiO_2 during the assembly synthesis process, the nano-SnO_2/SiO_2 assemblies with different weight ratios of SnO_2/SiO_2 (1:10, 3:10, 7:10, 13:10, 17:10, 10:20 and 30:10) were obtained.

Sb-doped nano-SnO_2/SiO_2 mesoporous assemblies were synthesized as follows. $SbCl_3{\cdot}5H_2O$ and $SnCl_4{\cdot}5H_2O$ were dissolved in acetylacetono with the molar ratio of 8:100. And then, E_tOH was added into the solution by stirring to get the precursor solution. The molar concentrations of $SnCl_4$ in the precursor solutions are 0.1, 0.5 and 2 M, respectively. Finally, these solutions were, respectively, mixed with the SiO_2 sols to prepare the dry gels containing Sb element, SnO_2 and SiO_2. The dry gel preparation route is the same as the above-mentioned step. Several parts of the dry gel were annealed at 300 °C in O_2 atmosphere (50% O_2 volume) for 2 h. Then, these dry gels were annealed at 500, 650, 800 and 950 °C for 1.5 h, respectively, by which the Sb-doped nano-SnO_2/SiO_2 mesoporous assemblies were finally obtained. During annealing, each part of dry gel corresponds to one temperature.

* Corresponding author. Tel.: +86 027 67885098; fax: +86 027 67885098.
E-mail address: chjyan2005@126.com (C. Yan).

0925-8388/$ – see front matter. Published by Elsevier B.V.
doi:10.1016/j.jallcom.2009.08.137

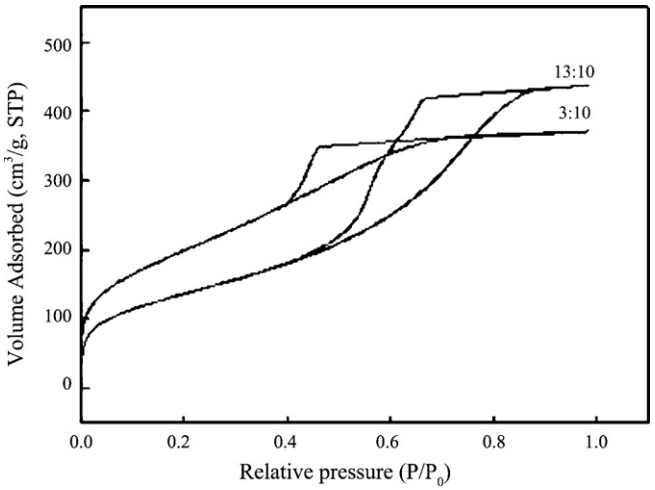

Fig. 1. N_2 adsorption–desorption isotherms of 3:10- and 13:10-nano-SnO_2/SiO_2 assemblies.

The Pd-doped nano-SnO_2/SiO_2 assemblies were synthesized as follows: $SnCl_4{\cdot}5H_2O$ and $PdCl_2$ were dissolved in the E_tOH aqueous solution by stirring. The molar ratio of $PdCl_2$:$SnCl_4$:E_tOH:H_2O is 0.1:1:2:8. Then, this solution with a certain weight of the SnO_2 sol was mixed under stirring for 30 min. After that, the mixed sol was put in a glassware to prepare the dry gels. The preparation route is the same as the above-mentioned step of the synthesis of dry SiO_2 gels. Finally, the dry gels were annealed at 300 °C in O_2 atmosphere (50% O_2 volume) for 2 h, followed by annealing at 650 °C for 1.5 h. As a result, Pd-doped nano-SnO_2/SiO_2 assemblies were obtained, in which the molar ratio of Pd:Sn is 1:10 and the weight ratio of SnO_2:SiO_2 is 3:10.

2.2. Characterization

The nitrogen adsorption–desorption isotherms were measured on an Omnisorp-100cx analyzer. The XRD patterns for nano-SnO_2/SiO_2 mesoporous assemblies were recorded on a (Philips X'Pert Pro MPD) X-ray diffractometer with Cu K_α radiation. The XPS spectra measurement was carried out on an X-ray photoelectronic energy spectrometer (type thermo ESCALAB 250). The optical absorption in the wavelength range of ultraviolet to near-infrared was measured on a (type Cary 5 E UV–vis) spectrometer.

3. Results and discussion

Fig. 1 shows N_2 adsorption–desorption isotherms of nano-SnO_2/SiO_2 assemblies. For nano-SnO_2/SiO_2 assemblies with the weight ratios of 3:10 and 13:10, respectively (3:10-nano-SnO_2/SiO_2

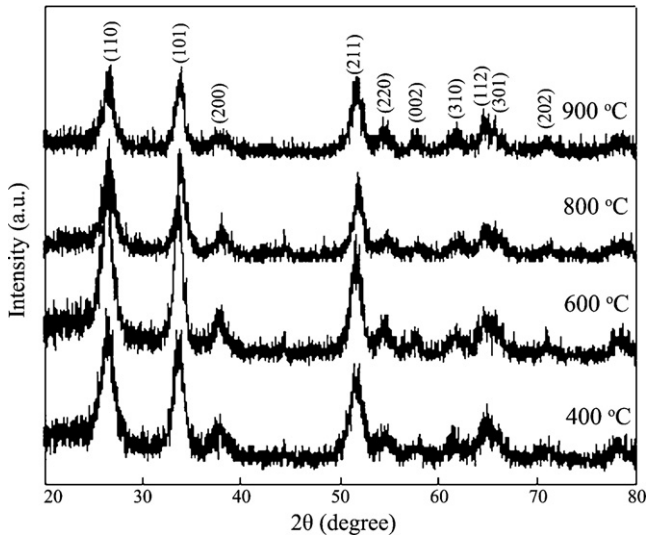

Fig. 2. XRD spectra of 5:10-nano-SnO_2/SiO_2 assemblies annealed at 400, 600, 800 and 900 °C, respectively.

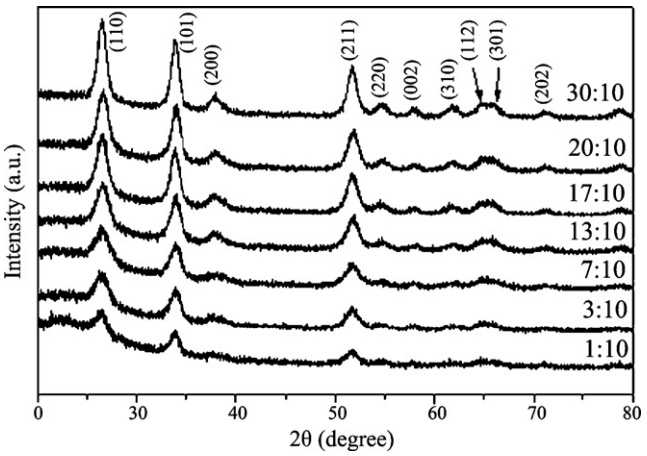

Fig. 3. XRD spectra of nano-SnO_2/SiO_2 assemblies annealed at 600 °C. The weight ratios of SnO_2:SiO_2 are 1:10, 3:10, 7:10, 13:10, 17:10, 20:10 and 30:10, respectively.

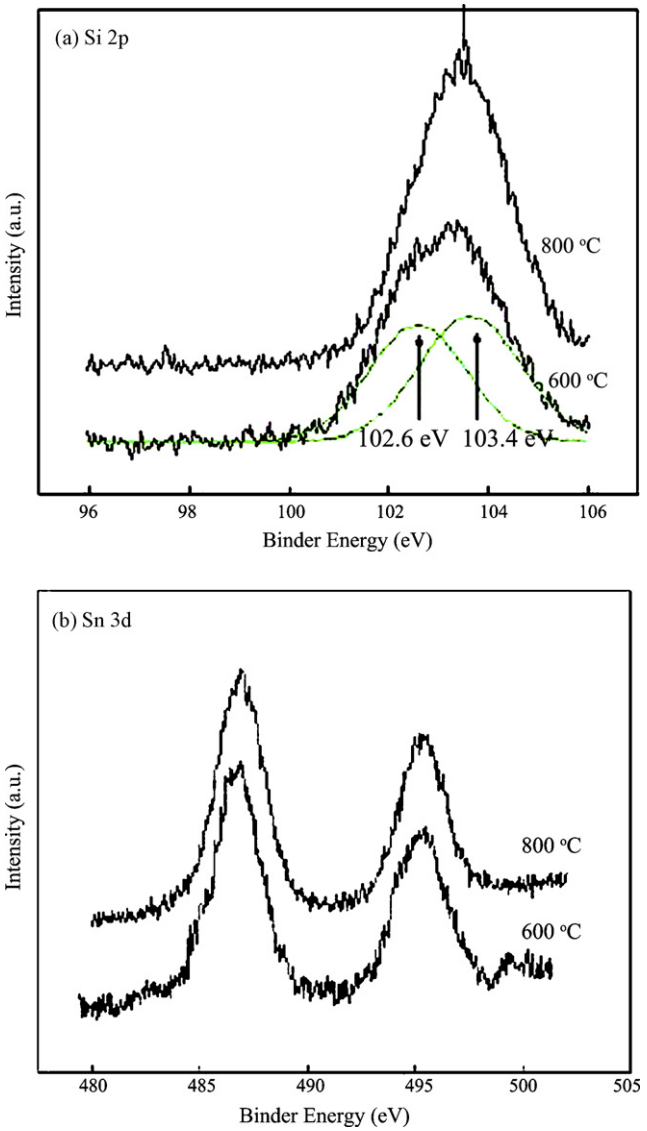

Fig. 4. (a) Si 2p XPS spectra of 13:10-nano-SnO_2/SiO_2 assemblies annealed at 600 and 800 °C, respectively; (b) Sn 3d XPS spectra of 13:10-nano-SnO_2/SiO_2 assemblies annealed at 600 and 800 °C, respectively.

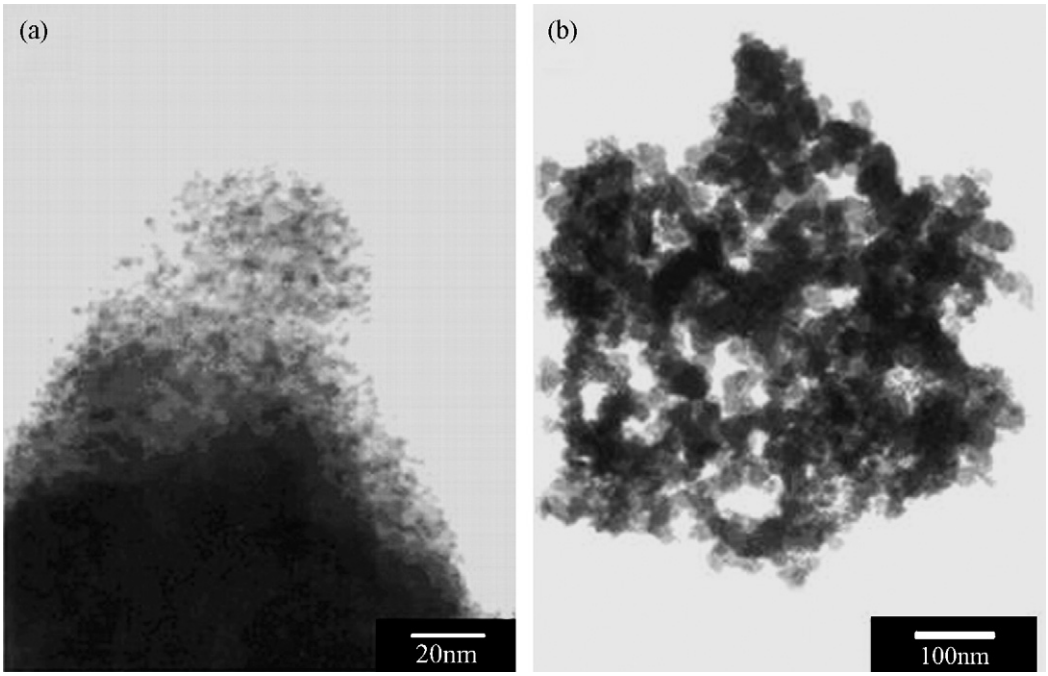

Fig. 5. (a) TEM photographs of 3:10-nano-SnO_2/SiO_2; (b) TEM photographs of 13:10-nano-SnO_2/SiO_2 assemblies.

assembly and 13:10-nano-SnO_2/SiO_2 assembly), both the N_2 adsorption–desorption isotherms exhibit the type IV characteristic, which is the direct evidence of the presence of mesopores. The hysteresis loop of the N_2 adsorption–desorption isotherm of the samples is type H_2. It indicates that there is a uniform pore diameter distribution. For Sb- and Pd-doped nano-SnO_2/SiO_2 assemblies, the N_2 adsorption–desorption isotherms are the same as that of the nano-SnO_2/SiO_2 assembly. Therefore, in this paper, the isotherms are not presented.

Fig. 2 displays X-ray diffraction spectra of 5:10-nano-SnO_2/SiO_2 assemblies annealed at 400, 600, 800 and 900 °C, respectively. All diffraction peaks belong to the diffraction peaks of SnO_2. The SiO_2 gives an amorphous background. It can be seen that with the increase of the annealed temperature, the peak width narrows. And as the annealed temperature increases from 800 to 900 °C, the peak height decreases. These results demonstrate that larger SnO_2 crystallines form and the crystalline number decreases with the increase of the annealed temperature due to SnO_2 particle aggregation formation. Fig. 3 gives the XRD spectra of nano-SnO_2/SiO_2 annealed at 600 °C. The weight ratios of SnO_2:SiO_2 are 1:10, 3:10, 7:10, 13:10, 17:10, 20:10 and 30:10, respectively. Clearly, with increasing the weight ratio of SnO_2:SiO_2, the diffraction peaks of SnO_2 become high and narrow. This is because under high SnO_2 concentration, the SnO_2 particles are easy to agglomerate to form large and more crystallines, but under the low SnO_2 concentration, the SnO_2 particles present good dispersion, so that the probability of SnO_2 particles forming larger crystallines decreases, resulting in forming wider and low X-ray diffraction peaks.

Si 2p and Sn 3d XPS spectra of 13:10-nano-SnO_2/SiO_2 assemblies after annealing at 600 and 800 °C are shown in Fig. 4(a) and (b), respectively. After annealing at 600 °C, the Si 2p XPS spectrum exhibits the double peaks in Fig. 4(a). By using Gauss simulating, the two peak positions correspond to the 2p electron binding energy of SiO_4 and SiO_x ($x < 4$), respectively. When the annealed temperature increases to 800 °C, the peak correspond to SiO_x ($x < 4$) disappeared and only the peak corresponding to the SiO_4 can be observed. This implies that SiO_x converted to SiO_4. The Sn 3d XPS spectra of 13:10-nano-SnO_2/SiO_2 assemblies obtained by annealing at 600 and 800 °C, respectively, are displayed in Fig. 4(b). It is clear that for different annealing temperatures the difference of two Sn 3d XPS spectra is very small. The Sn $3d_{5/2}$ and Sn $3d_{3/2}$ electron binding energy at the two peak positions for the assembly after annealing at 600 °C is lower than that after annealing at 800 °C. And the former peak symmetry is lower. This indicates that the Sn match in the assembly after annealing at 600 °C is not saturated, and unstable SnO and Sn_3O_4 exist in the assembly.

The TEM photographs of 3:10- and 13:10-nano-SnO_2/SiO_2 assemblies are given in Fig. 5(a) and (b), respectively. It can be seen that the black SnO_2 particles distribute in the pores of grey SiO_2 mesoporous solids. For 3:10-nano-SnO_2/SiO_2 assemblies the diameters of SnO_2 particles are 4–10 nm. For 13:10-nano-SnO_2/SiO_2 assemblies large numbers of SnO_2 particles connect each other to form a network structure in the mesoporous SiO_2 solid, as shown in Fig. 5(b) and the diameters of SnO_2 particles are 20–30 nm. The above result demonstrates that with increasing SnO_2 amount the diameter of the SnO_2 crystalline increases. And especially, when the SnO_2 network forms, these assemblies possess good heat transfer ability.

The Pd- and Sb-doped SnO_2 have been reported [25,26], however, most of the study are focused on the effect of the dopants on its conductivity. In this paper, we studied the optical absorption properties. Fig. 6 shows the optical absorption spectra of the Sb-doped 3:10-nano-SnO_2/SiO_2 assembly, the Pd-doped 1:10-nano-SnO_2/SiO_2 assembly and the 1:10-nano-SnO_2/SiO_2 assembly, respectively, after annealing at 650 °C for 1.5 h. It is clear that only Sb-doped sample exhibits a strong near-infrared absorption step and other two samples almost do not absorb near-infrared light in the wavelength range from 300 to 1500 nm. This implies that enhanced near-infrared absorption can be attributed to Sb doping.

Fig. 7 displays the optical absorption spectra of the Sb-doped 3:10-nano-SnO_2/SiO_2 assemblies annealed at 500, 650, 800, and 950 °C for 1.5 h, respectively, in the wavelength range from 300 to 1500 nm. It can be observed that with the increase of annealing temperature, the slope sides of near-infrared absorption step shift to longer wavelength (red shift). With increasing the weight ratio of SnO_2/SiO_2 from 1:10 to 3:10 to 8:10, the slope side of near-infrared absorption step presents a "red shift", which has been shown in

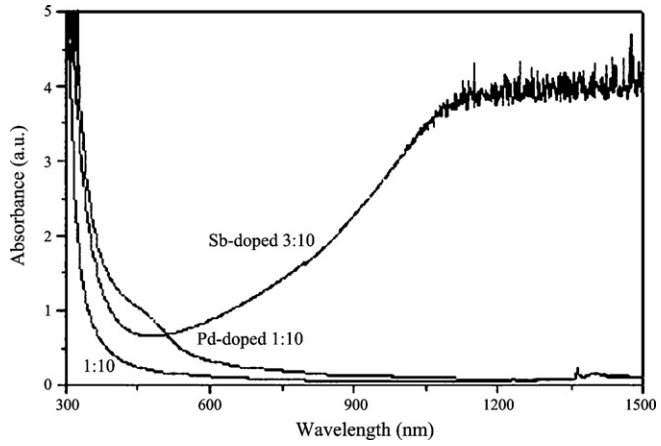

Fig. 6. Optical absorption spectra of Sb-doped 3:10-nano-SnO_2/SiO_2, Pd-doped 1:10-nano-SnO_2/SiO_2 and 1:10-nano-SnO_2/SiO_2 assemblies annealed at 650 °C for 1.5 h.

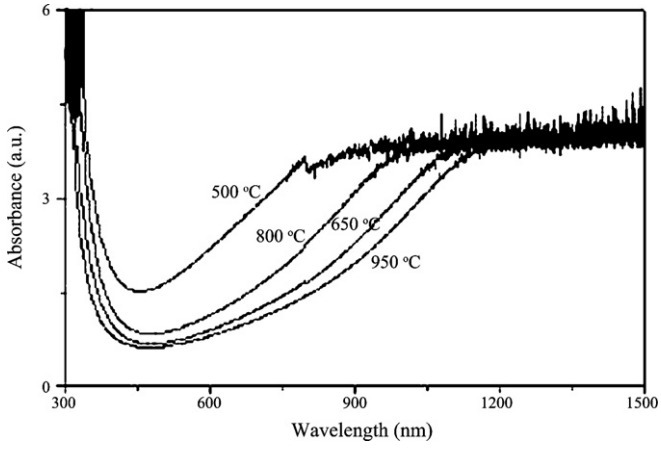

Fig. 7. Optical absorption spectra of Sb-doped 3:10-nano-SnO_2/SiO_2 assemblies annealed at 500, 650, 800 and 950 °C for 1.5 h, respectively.

Fig. 8. The "red shift" is caused by the size increase of SnO_2 leading to SnO_2 energy gap narrowing.

From Fig. 6, the near-infrared absorption band can be associated with deep level centers originated by the Sb introduced into the SnO_2 lattice, and a similar effect originated in CdTe:Ni in the presence of the transition metal impurities. For Sb-doped SnO_2 the Sb impurity energy levels form in the energy gap of SnO_2. Heo [24] demonstrated that the near-infrared absorption is attributed to impurity electron transition from the ground state to the excitation state. Therefore, it can be supposed that the near-infrared absorption originating from the electron transitions from the s orbit to the sp orbit in $Sb^{3\pm}$ ions [27,28].

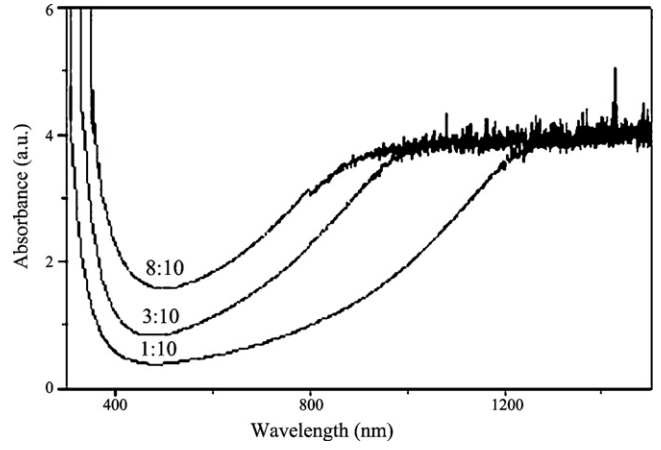

Fig. 8. Optical absorption spectra of Sb-doped 8:10-, 3:10-, 1:10-nano-SnO_2/SiO_2 assemblies annealed at 800 °C.

With increasing the annealing temperature or SnO_2 amount (increasing the weight ratio of SnO_2:SiO_2), as shown in Figs. 7 and 8, respectively, the slope side of the near-infrared absorption step presents "red shift". This phenomenon is caused by the SnO_2 crystalline growth, so that the quantum confinement effect decreases and thus the energy gap of SnO_2 become narrow. This makes the distances among the impurity energy levels become narrow. Therefore, the near-infrared absorption step slope exhibits "red shift".

4. Conclusions

In summary, the assemblies of nano-SnO_2/SiO_2 and Sb- or Pd-doped nano-SnO_2/SiO_2 were synthesized by a sol–gel route. The nano-SnO_2 particles are located in the pores of SiO_2 dry gels. Experimental results indicate that only Sb-doped nano-SnO_2/SiO_2 assemblies display a near-infrared absorption step in the optical absorption spectrum of the wavelength range of 300–1500 nm. The near-infrared absorption step appearance mechanism and the red shift reason of the near-infrared absorption step slope side in the optical absorption spectra with increasing SnO_2 crystalline diameters annealing temperature were discussed.

References

[1] A. Yilanci, I. Dincer, H.K. Ozturk, Prog. Energy Combust. 35 (2009) 231–244.
[2] D. Russo, C.M. Kown, C. Roger, J. Brotzman, J. Stricker, Thin Solid Films 398–399 (2001) 65–70.
[3] X. Fang, Y. Bando, M. Liao, U.K. Gautam, C. Zhi, B. Dierre, B. Liu, T. Zhai, T. Sekiguchi, Y. Koide, D. Golberg, Adv. Mater. 21 (2009) 2034–2039.
[4] X. Fang, Y. Bando, U.K. Gautam, C. Ye, D. Golberg, J. Mater. Chem. 18 (2008) 509–522.
[5] Y.S. Feng, R.S. Yao, L.D. Zhang, Chin. Phys. Lett. 21 (2004) 1374–1376.
[6] U.K. Gautam, X. Fang, Y. Bando, J. Zhan, D. Golberg, ACS Nano 2 (2008) 1015–1021.
[7] R. Koeppe, O. Bossart, G. Calzaferri, N.S. Sariciftci, Sol. Energy Mater. Sol. Cells 91 (2007) 986–995.
[8] F. Xia, E.C. Qu, L. Wang, J.Q. Wang, Dyes Pigments 76 (2008) 76–81.
[9] Y. Shen, J. Bao, N. Dai, J. Wu, F. Gu, J.C. Tao, J.C. Zhang, Appl. Surf. Sci. 255 (2009) 3908–3911.
[10] N.B. Lihitkar, M.K. Abyaneh, V. Samuel, R. Pasricha, S.W. Gosavi, S.K. Kulkarni, J. Colloid Interf. Sci. 314 (2007) 310–316.
[11] W.A. Badawy, J. Alloy Compd. 464 (2008) 347–351.
[12] S. Shanmugan, S. Balaji, D. Mutharasu, Mater. Lett. 63 (2009) 1189–1191.
[13] Y.B. Xu, Y.J. Tang, C.J. Li, G.H. Cao, W.L. Ren, H. Xu, Z.M. Ren, J. Alloys Compd. 481 (2009) 837–840.
[14] Z.M. Tian, S.L. Yuan, J.H. He, P. Li, S.Q. Zhang, C.H. Wang, Y.Q. Wang, S.Y. Yin, L. Liu, J. Alloy Compd. 466 (2008) 26–30.
[15] L.M. Fang, X.T. Zu, Z.J.L.S. Zhu, C.M. Liu, W.L. Zhou, L.M. Wang, J. Alloy Compd. 454 (2008) 261–267.
[16] J.F. Wang, H.C. Chen, W.B. Su, G.Z. Zang, B.W.W. Gao, J. Alloy Compd. 413 (2006) 35–39.
[17] D.P. Joseph, P. Renugambal, M. Saravanan, S.P. Raja, C. Venkateswaran, Thin Solid Films 517 (2009) 6129–6136.
[18] Y.D. Wang, T. Chen, Electrochim. Acta 54 (2009) 3510–3515.
[19] G.Q. Qin, D.C. Li, Z.W. Chen, Y.L. Hou, Z.J. Feng, S.M. Liu, Comput. Mater. Sci. 46 (2009) 418–424.
[20] B. Hadjarab, A. Bouguelia, A. Benchettara, M. Trari, J. Alloy Compd. 461 (2008) 360–366.
[21] A. Moadhen, C. Bouzidi, H. Elhouichet, R. Chtourou, M. Oueslati, Opt. Mater. 31 (2009) 1224–1227.
[22] P.I. Gaiduk, J. Chevallier, W. Wesch, A.N. Larsen, Nucl. Instrum. Methods Phys. Res. B 267 (2009) 1336–1339.
[23] Z.Z. Yuan, D.S. Li, Z.H. Liu, X.Q. Li, M.H. Wang, P.H. Cheng, P.L. Chen, D.R. Yang, J. Alloy Compd. 474 (2009) 246–249.
[24] J. Heo, J. Mater. Sci. Lett. 14 (1995) 1014–1016.
[25] D.R. Leite, I.O. Mazali, E.C. Aguiar, W.C. Las, M. Cilense, J. Mater. Sci. 41 (2006) 6256–6259.
[26] A. Kolmakov, D.O. Klenov, Y. Lilach, S. Stemmer, M. Moskovits, Nano Lett. 5 (2005) 667–673.
[27] M. Fang, X.L. Tan, X.L. Cao, L.D. Zhang, P.S. Liu, Z. Jiang, J. Phys. D: Appl. Phys. 40 (2007) 7648–7651.
[28] M. Fang, X.L. Tan, B.C. Cheng, L.D. Zhang, J. Mater. Chem. 19 (2009) 1320–1324.